

Review

Comprehensive Analysis of HY-2B/2C/2D Satellite-Borne GPS Data Quality and Reduced-Dynamic Precise Orbit Determination

Xin Jin ^{1,2,3}, Guangzhe Wang ³ , Jinyun Guo ^{3,*} , Hailong Peng ^{4,5}, Yongjun Jia ^{4,5}  and Xiaotao Chang ⁶

¹ Faculty of Geomatics, Lanzhou Jiaotong University, Lanzhou 730070, China; xinjin@lzjtu.edu.cn

² National-Local Joint Engineering Research Center of Technologies and Applications for National Geographic State Monitoring, Lanzhou 730070, China

³ College of Geodesy and Geomatics, Shandong University of Science and Technology, Qingdao 266590, China; wangguangzhe@sdust.edu.cn

⁴ National Satellite Ocean Application Service, Beijing 100081, China; phl@mail.nsoas.org.cn (H.P.); jiyongjun@mail.nsoas.org.cn (Y.J.)

⁵ Key Laboratory of Space Ocean Remote Sensing and Application, Ministry of Natural Resources, Beijing 100081, China

⁶ Land Satellite Remote Sensing Application Center, Ministry of Natural Resources, Beijing 100048, China; cxt@lasac.cn

* Correspondence: guojy@sdust.edu.cn

Abstract: The deployment of the HY-2B/2C/2D satellite constellation marks a significant advancement in China's marine dynamic environmental satellite program, forming a robust three-satellite network. All satellites are equipped with the "HY2_Receiver", an indigenous technological achievement. Precise orbit determination using this receiver is critical for monitoring dynamic oceanic parameters such as sea surface wind fields and heights. This study presents a detailed analysis and comparison of the GPS data quality from the HY-2B/2C/2D satellites, emphasizing the impact of phase center variation (PCV) model corrections on orbit accuracy, with a particular focus on high-precision reduced-dynamic orbit determination. The experimental results demonstrate that the GPS data from the satellites exhibit consistent satellite visibility and minimal multipath errors, confirming the reliability and stability of the receivers. Incorporating PCV model corrections significantly enhances orbit accuracy, achieving improvements of approximately 0.3 cm. Compared to DORIS-derived orbits from the Centre National d'Études Spatiales (CNES), the GPS-derived reduced-dynamic orbits consistently reach radial accuracies of 1.5 cm and three-dimensional accuracies of 3 cm. Furthermore, validation using Satellite Laser Ranging (SLR) data confirms orbit accuracies better than 3.5 cm, with 3D root mean square (RMS) accuracies exceeding 3 cm in the radial (R), along-track (T), and cross-track (N) directions. Notably, the orbit determination accuracy remains consistent across all satellites within the HY-2B/2C/2D constellation. This comprehensive analysis highlights the consistent and reliable performance of the indigenous "HY2_Receiver" in supporting high-precision orbit determination for the HY-2B/2C/2D constellation, demonstrating its capability to meet the rigorous demands of marine dynamic environmental monitoring.

Keywords: HY-2B/2C/2D; satellite-borne GPS; reduced-dynamic orbit determination; data quality analysis; antenna phase center change



Academic Editors: Marco Zannoni and Giacomo Lari

Received: 7 December 2024

Revised: 26 January 2025

Accepted: 28 January 2025

Published: 30 January 2025

Citation: Jin, X.; Wang, G.; Guo, J.; Peng, H.; Jia, Y.; Chang, X.

Comprehensive Analysis of HY-2B/2C/2D Satellite-Borne GPS Data Quality and Reduced-Dynamic Precise Orbit Determination.

Aerospace **2025**, *12*, 102. <https://doi.org/10.3390/aerospace12020102>

Copyright: © 2025 by the authors.

Licensee MDPI, Basel, Switzerland.

This article is an open access article distributed under the terms and conditions of the Creative Commons Attribution (CC BY) license

(<https://creativecommons.org/licenses/by/4.0/>).

1. Introduction

The HY-2B/2C/2D satellite constellation is a crucial component of China's marine dynamic environmental monitoring program. Since the successful launch of the HY-2D

satellite on 19 May 2021, the three satellites (HY-2B, HY-2C, and HY-2D) have collectively formed China's first marine dynamic environmental satellite monitoring network. With this satellite constellation, the global ocean observation cycle has been reduced from over 20 days for a single satellite to just 6 h, achieving a coverage capacity of more than 80% for global ocean monitoring. This has significantly enhanced the timeliness and accuracy of ocean monitoring [1]. The network is capable of simultaneously retrieving multiple high-temporal-resolution marine dynamic environmental parameters, such as sea surface wind fields, wave heights, sea surface heights, and sea surface temperatures, establishing a comprehensive observation system for all-weather, all-time, and global ocean efficient detection [2].

The satellite constellation not only improves observational capabilities but also enhances data diversity and high precision. The HY-2 series satellites are equipped with advanced instruments such as microwave scatterometers and radar altimeters for collecting critical marine environmental data. They are also equipped with DORIS receivers [3], laser reflector arrays [4], and the independently developed 'HY2_Receiver' onboard GPS receiver to ensure precise orbit determination. The high-precision orbit data obtained via the GNSS receiver supports precise satellite orbit control and enables gravity field model inversion, further advancing research in ocean dynamics and climate change [5]. Additionally, the satellite constellation has the capability for polar and oceanic observations, with sun-synchronous orbits ensuring polar marine environment monitoring and non-sun-synchronous orbits effectively separating tidal components to address tidal aliasing issues. Through constellation-based observation, the variety of satellite data products has been enriched, further enhancing the application efficiency in China's coastal regions and providing essential support for the development of high-resolution regional marine dynamic environmental data products.

The use of satellite-borne GPS receivers for precise orbit determination has been integral to satellite missions since the successful POD experiment using GPS data from the Topex/Poseidon satellite in 1992 [6]. These GPS receivers have been deployed on multiple low-Earth-orbit (LEO) satellites, and owing to their advantages of high precision, all-weather operability, and continuous data acquisition, they have become the primary technology for determining the precise orbits of LEO satellites [7–10]. The orbit determination methods employing satellite-borne GPS [11] encompass kinematic, dynamic, and reduced dynamic methods. Among these, the reduced dynamic method effectively harnesses satellite geometric observations and dynamic model information. It compensates for dynamic model limitations by employing pseudo-random pulse parameters, making it the most widely adopted method for the orbit determination of LEO satellites [12]. Recent research by Wang et al. [13] identified potential periodicity in empirical acceleration for HY-2B, leading to an improved empirical acceleration model. Guo et al. [7] introduced a novel method for verifying orbit accuracy using DORIS data, with the results indicating an external validation accuracy of 6.3 mm/s for HY-2C reduced-dynamic (RD) orbits.

The quality of satellite data is a critical factor impacting precise orbit determination and serves as a key benchmark for assessing receiver quality [14]. In theory, observation data errors should manifest as noise sequences with small variances and zero means. However, actual GPS data incorporates unmodeled errors, which can significantly influence orbit determination results. Key indicators used to assess the quality of satellite-borne GPS data include satellite visibility, multipath effects, data integrity, and more [15]. Hwang et al. [16] conducted an analysis of GPS data quality for F3/C and GRACE satellites, highlighting that larger multipath errors can lead to cycle slips, an increased number of estimated parameters during orbit determination, and ultimately reduced orbit determination accuracy. Phase center variation (PCV) represents a notable error source affecting orbit determination accu-

racy [17,18]. While prior PCV values can be obtained before the launch, the complexities of satellite launch, including forces and fuel consumption, result in actual PCV values changing. Therefore, high-precision orbit determination necessitates the consideration of in-orbit PCV estimation [19,20].

Currently, a comprehensive investigation comparing the orbit determination accuracy of HY-2B/2C/2D satellites is lacking. Building upon satellite-borne GPS data, this paper conducts a systematic exploration of reduced-dynamic precision orbit determination for HY-2B/2C/2D satellites. This exploration encompasses the analysis of observation data quality, precision orbit determination strategies and models, and orbit determination accuracy. The second section introduces fundamental information regarding the HY-2B/2C/2D satellites, including their attitude dynamics. Section 3 delves into an analysis of the quality of satellite-borne GPS data through metrics such as multipath errors, satellite altitude angles, and satellite visibility, providing insights into receiver performance. Section 4 discusses the influence of in-orbit PCV estimation on orbit determination. The orbit determination strategy is introduced, and the accuracy of reduced-dynamic orbit is evaluated from overlapping orbit validation, a comparison with Centre National d'Études Spatiales (CNES) orbits, Satellite Laser Ranging (SLR) orbit validation, and so on. Section 5 is the conclusion.

2. HY-2B/2C/2D Spacecraft

To provide a more comprehensive understanding of the orbit performance and accuracy of the satellite-borne GPS receiver, “HY2_Receiver,” developed in China, we shall commence with a concise introduction of the HY-2B/2C/2D satellites and their associated attitude characteristics.

2.1. Satellite Introduction

The HY-2B/2C/2D satellite constellation offers the capability for global continuous observation, enabling real-time data collection within the region spanning from 5° S to 50° N and 100° E to 150° E. These satellites actively transmit real-time remote sensing microwave signals and receive the reflected remote sensing signals.

The HY-2B satellite orbits in a sun-synchronous frozen orbit, characterized by an inclination of 99.3° and an orbital altitude of 973 km. In contrast, the HY-2C and HY-2D satellites follow regression frozen orbits with inclinations of 66° and orbital altitudes of 1336 km and 973 km, respectively. Specific orbital information is summarized in Table 1.

Table 1. HY-2B/2C/2D satellite information.

Satellite	HY-2B	HY-2C	HY-2D
Launch time	25 October 2018	21 September 2020	19 May 2021
Orbit type	Sun-synchronous orbit	Regression Frozen orbit	Regression Frozen orbit
Orbital altitude	973 km	1336 km	973 km
Orbital inclination	99.3°	66°	66°
Mass at launch	1500 kg	1500 kg	1575 kg
Repeat period	14 day	10 day	10 day
Adjacent orbit pitch:	207.64 km	292.52 km	292.52 km

All HY-2 satellites are equipped with a satellite-borne DORIS receiver, a laser retro-reflector arrays, and the indigenously developed “HY2_Receiver” satellite-borne GPS receiver. The receiver uses non-coding tracking technology, capable of tracking GPS signals on L1 and L2 frequencies, achieving centimeter-level orbit accuracy [21].

Figure 1 depicts the distribution of these payloads in the satellite coordinate system, with the +X axis oriented in the direction of flight, the +Z axis aligned with the geocentric direction, and the +Y axis orthogonal to both the X and Z axes, forming a right-handed coordinate system [22].

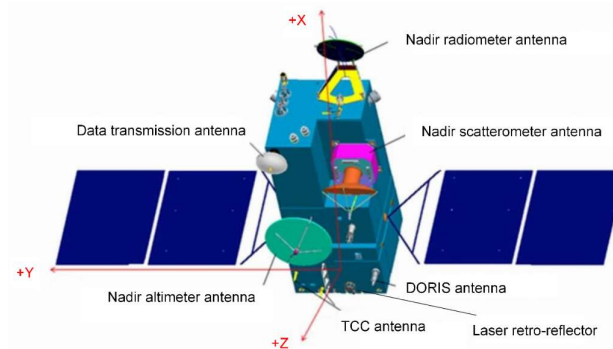


Figure 1. Satellite and its payloads.

2.2. Attitude Data

The attitude of the HY-2B/2C/2D satellites plays a critical role in precise orbit determination (POD) as it directly affects the transformation from the satellite coordinate system to the orbital coordinate system. This transformation is crucial for correctly processing GPS observational data and applying phase center variation (PCV) corrections. When the satellite is in the zero attitude, the orbital coordinate system coincides with the satellite coordinate system.

The satellite attitude is represented by three Euler angles [23], namely yaw angle, roll angle, and pitch angle around the X, Y, and Z axes shown in Figure 1. The rotation matrix is calculated from the Euler angles to obtain the transformation matrix from the satellite coordinate system to the orbital coordinate system, and the rotation matrix is shown in Equation (1):

$$R = \begin{bmatrix} \cos \varphi \cos \beta & \sin \theta \sin \varphi \sin \beta - \cos \theta \sin \varphi & \cos \theta \sin \varphi \cos \beta + \sin \theta \sin \beta \\ \cos \varphi \sin \beta & \sin \theta \sin \varphi \cos \beta + \cos \theta \cos \beta & \cos \theta \sin \varphi \sin \beta - \sin \theta \cos \varphi \\ -\sin \varphi & \sin \theta \cos \varphi & \cos \theta \cos \beta \end{bmatrix} \quad (1)$$

where R is conversion matrix, and φ , β , and θ are the yaw angle, roll angle, and pitch angle, respectively.

To gain a more intuitive understanding of the relationship between the satellite coordinate system and the orbital coordinate system (attitude), we have depicted attitude figures for the HY-2B/2C/2D satellites, as shown in Figure 2. The figure shows the attitude angles (sampling interval 1 s) of the 2020 DOY350 HY-2B/2C satellite and the 2021 DOY263 HY-2D satellite. It can be seen that the attitude of the HY-2B satellite shows limited variations, and the yaw angle of the HY-2C satellite is large but stable. However, the yaw angle of the HY-2D satellite is large and exhibits a variation of 70° . It is important to note that the HY-2B/2C/2D satellites maintain non-zero attitudes during their operation. Consequently, the attitude data are crucial for the conversion from the satellite coordinate system to the orbital coordinate system.

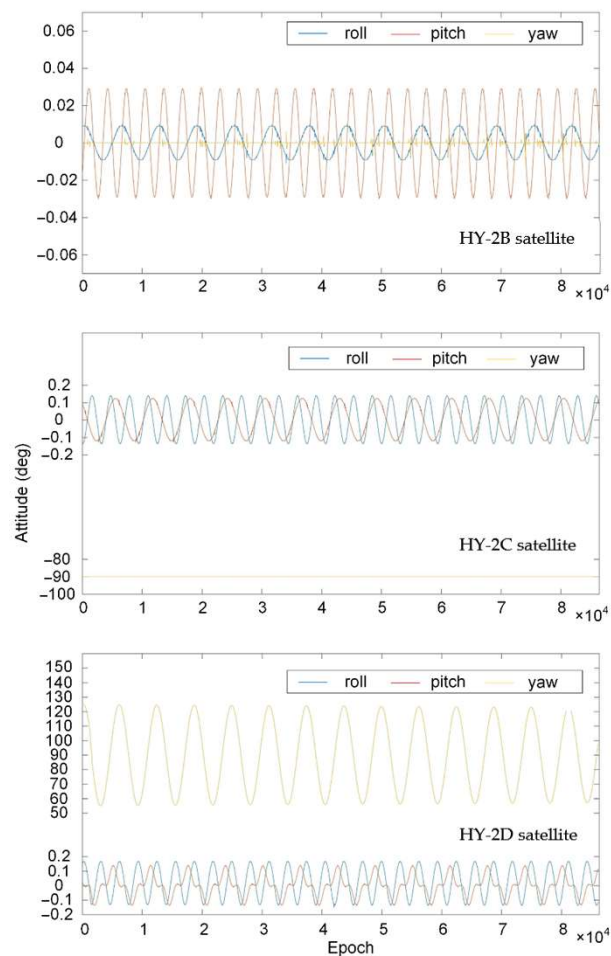


Figure 2. Attitude variation features of HY-2B/2C/2D satellites.

3. Satellite-Borne GPS Data Quality Analysis

LEO satellites move at high velocities and operate in complex environmental conditions. The quality of satellite observation data plays a pivotal role in achieving precise orbit determination. Consequently, it is imperative to conduct a thorough analysis of observation data quality, as it directly reflects the receiver's performance. This analysis primarily relies on indicators such as the number of visible satellites, multipath error, data integrity rate, and other relevant metrics.

In this regard, we meticulously examine the quality of satellite-borne GPS data, aiming to assess the transmission capabilities and operational status of the "HY2_Receiver". This assessment forms a crucial foundation for the ongoing development of indigenous GPS receivers, offering valuable scientific insights. To delve into these indicators in a comprehensive manner, we employ TEQC [24] as our analytical tool.

In this study, the on-board GPS data from the HY-2B and HY-2C satellites (2020 DOY349-355) and the HY-2D satellite (2021 DOY263-269) were used for experiments. While the data acquisition periods differ, Figure 3 shows that the solar F10.7 index exhibits a similar overall trend during both time periods. Although there are some variations, such as a peak in September 2021 compared to a relatively low level in December 2020, these differences are negligible and have an almost identical impact on the precise orbit determination of the HY-2B/2C/2D satellites [25].

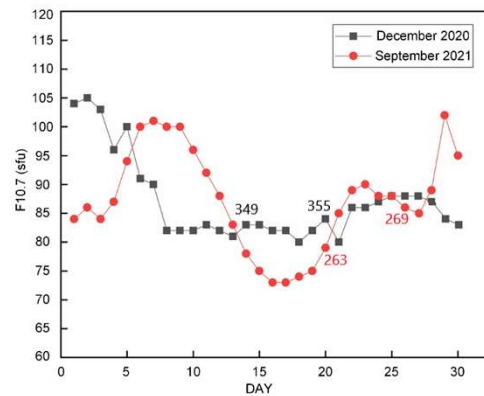


Figure 3. Change in F10.7 values.

3.1. Satellite Visibility

Satellite visibility refers to the count of satellites tracked by the receiver during a specific epoch, and it serves as an indicator of the receiver’s ability to track GPS satellites effectively. In the precise orbit determination process, having a greater number of observations can enhance the accuracy of the parameters being estimated. When more satellites are observed, it provides additional redundant observations, thereby further improving the accuracy of the solution.

The satellite-borne GPS data from the HY-2B and HY-2C satellites in 2020 DOY349–355 and HY-2D satellite in 2021 DOY263–269 were used for experimental analysis. Figure 4 illustrates the distribution characteristics of the number of satellites observed by the receiver. Notably, 99.7% of the epoch can observe four or more satellites, while 95.5% of the epoch enabled the observation of five or more satellites. Moreover, in 73.4% of the epoch, six or more satellites were observed. In contrast, only 0.3% of the epoch had fewer than four satellites observed. A majority of the available satellites during these observations fell within the range of 5 to 8 satellites. These findings underscore that the “HY2_Receiver” is fully capable of meeting the requirements for high-precision orbit determination and exhibits reliable and stable performance.

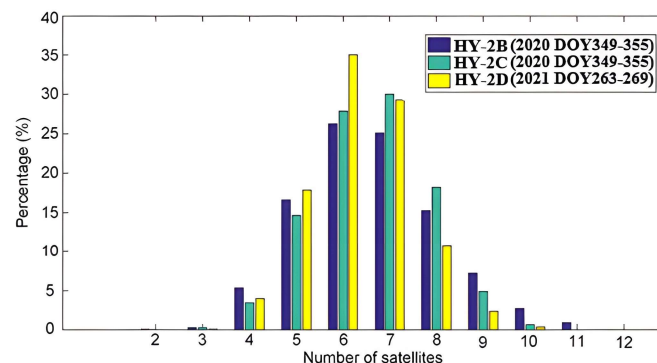


Figure 4. Number of single epoch observation satellites.

The HY-2B/2C/2D satellite-borne GPS observation data encompass five data types: C1C, C1P, C2P, L1C, and L2P. The number and percentage of missing data for each data type during the experiment (sampling rate 1 s) were counted. From Table 2, it can be found that the missing amount of C1C, C1P, and L1C observational data in L1 band is significantly less than that of C2P and L2P observational data in L2 band. This indicates that the “HY2_Receiver” can receive the L1 band signal better.

Table 2. Statistics of missing observational data.

	C1C	C1P	C2P	L1C	L2P
HY-2B missing amount	3592	114,359	217,844	14,652	228,309
HY-2B missing percent	0.09%	2.85%	5.42%	0.36%	5.69%
HY-2C missing amount	2818	123,452	226,025	9955	233,007
HY-2C missing percent	0.07%	3.15%	5.76%	0.25%	5.94%
HY-2D missing amount	2146	117,773	204,863	8807	211,108
HY-2D missing percent	0.06%	3.14%	5.47%	0.24%	5.63%

3.2. Multipath Error

During the propagation of satellite signals, external factors in the surrounding environment can lead to the phenomenon known as multipath effect. This effect occurs when reflected signals become superimposed on the direct satellite signals received by the receiver. In our analysis, we investigated the multipath errors present in the HY-2B/2C/2D satellite-borne GPS data during our experiment. Figure 5 provides a visual representation of the temporal variations in multipath errors in the L1 and L2 bands. Notably, the time-frames when significant errors in MP1 (multipath error in L1) and MP2 (multipath error in L2) occur are nearly identical.

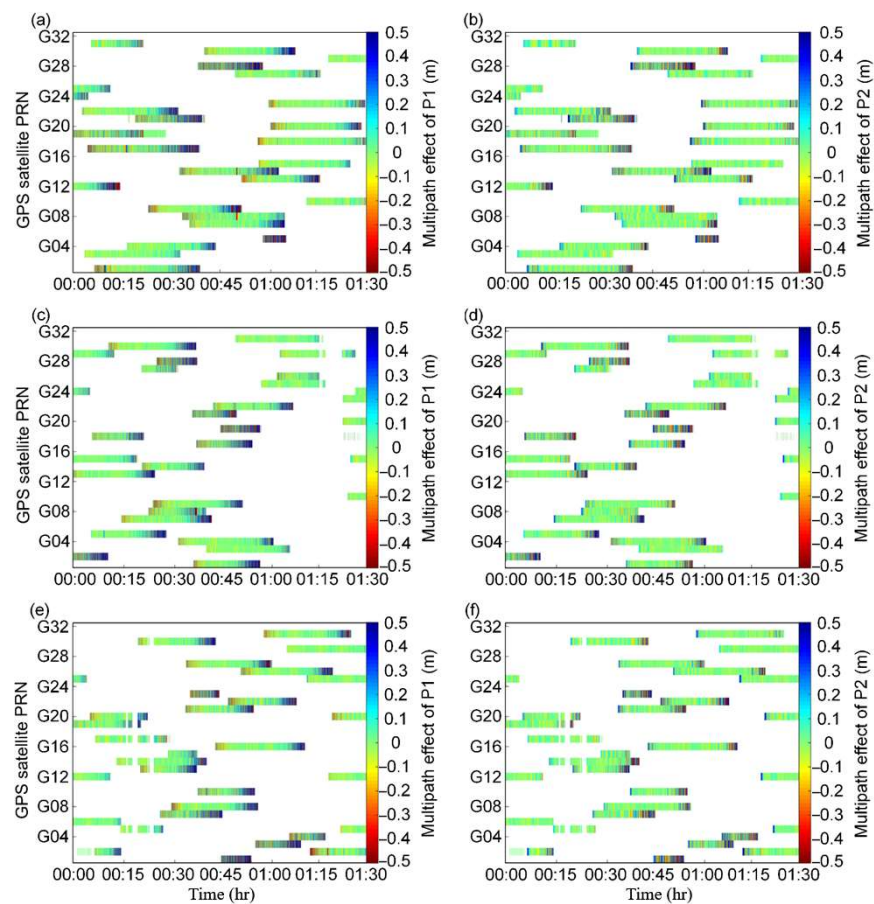


Figure 5. Multipath error ((a) HY-2B satellite MP1, (b) HY-2B satellite MP2, (c) HY-2C satellite MP1, (d) HY-2C satellite MP2, (e) HY-2D satellite MP1, (f) HY-2D satellite MP2).

Based on the linear combination of pseudo-range and carrier phase data, the multipath errors in L1 and L2 bands can be calculated by ignoring the effect of measurement noise [26]:

$$\begin{aligned}
 MP1 &= M_1 - \left(1 + \frac{2}{\alpha-1}\right)\varphi_1 + \left(\frac{2}{\alpha-1}\right)\varphi_2 \\
 MP2 &= M_2 - \left(\frac{2\alpha}{\alpha-1}\right)\varphi_1 + \left(\frac{2\alpha}{\alpha-1} - 1\right)\varphi_2
 \end{aligned}
 \tag{2}$$

where $MP1$ and $MP2$ represent the multipath errors of two frequencies; M_1 and M_2 are the pseudorange observations of the two frequencies; φ_1 and φ_2 are the carrier phase observations of the two frequencies; and $\alpha = f_1/f_2$, where f_1 and f_2 are the frequencies of the two bands.

To better illustrate the multipath effect, data from the first one and a half hours before the first day of each satellite experimental period were selected for multipath error analysis, and the results are shown in Figure 5. From the observations made in Figure 5, it is evident that the $MP1$ values are slightly higher than the $MP2$ values. The multipath errors for most satellites display minimal fluctuations and only exhibit significant changes during the early and late stages of GPS satellite signal reception. Notably, lower elevation angles have a more pronounced impact on $MP1$, leading to more substantial fluctuations in $MP1$ compared to $MP2$ during the initial and final phases of signal reception. However, in the middle of signal reception, both $MP1$ and $MP2$ values become smaller and more stable, primarily due to the higher elevation angle.

Table 3 summarizes the quality indicators of HY-2B/2C/2D satellite-borne GPS data, including multipath error, average elevation angle, and satellite visibility. The root mean square (RMS) average values for multipath errors in the L1 band for HY-2B/2C/2D satellites are 0.36 m, 0.38 m, and 0.34 m, respectively. In the L2 band, the RMS average values for multipath errors are 0.24 m, 0.27 m, and 0.22 m, respectively. Given that the surface environment of the satellites remains largely consistent, there are no significant variations in the average elevation angle, multipath error, and satellite visibility. This uniformity in the quality of satellite-borne GPS data across HY-2B/2C/2D satellites highlights that the “HY2_Receiver” operates effectively and reliably.

Table 3. Multipath error RMS value and mean elevation angle.

Satellite	MP1 (m)	MP2 (m)	Mean Elevation Angle (°)	Satellites Visibility
HY-2B	0.36	0.24	33.1	6.7
HY-2C	0.38	0.27	35.6	6.6
HY-2D	0.34	0.22	34.8	6.4

4. Satellite Precision Orbit Determination and Accuracy Analysis

4.1. Orbit Determination Strategy

In this study, we utilized Bernese 5.2 to perform precision orbit determination for HY-2B/2C/2D satellites [27], and the orbit determination arc was set to 24 h. The reduced dynamic method can combine the advantages of dynamic method and kinematic method [28–30], and adding the dynamic model weakens the influence of conservative and non-conservative forces. This method employs empirical parameters and pseudo-random pulses, enabling it to better accommodate dynamic model errors and residual perturbation effects [31–34].

The orbit determination strategy is shown in Table 4. The empirical parameters are used to absorb non-conservative forces such as solar radiation and atmospheric resistance. To address dynamic model errors, a set of pseudo-random pulses were introduced at intervals of 6 min in the R, T, and N directions. These pseudo-random pulses had a prior standard deviation of 5 nm/s^2 [35].

Table 4. Reduced-dynamic orbit determination strategy of HY-2B/2C/2D satellites.

Model/Parameters	Description
Global Gravity Field Model	XGM2019 [36]
N-body	JPL DE405 [37]
Solid-earth tides	TIDE2000
GPS antenna phase center variation	PCV.I14
Ocean Tides	FES2014 [38]
Elevation cutoff	5°
Sampling interval	1 s
GPS orbit	CODE precision orbit (15 min)
GPS precise clock offset	CODE precise clock offset (30 s)

4.2. Influence of PCV on HY-2B/C/D Satellite Orbit Determination

While it is possible to measure a priori PCV values for LEO satellites prior to launch, the satellite's flight environment, influenced by factors such as atmospheric pressure and temperature, significantly deviates from the ground environment. This leads to notable disparities between the actual PCV values in orbit and the a priori PCV values determined on the ground. Consequently, in-orbit PCV estimation holds pivotal significance for achieving precise orbit determination of the satellite.

The main estimation methods of the LEO satellite antenna PCV model include the direct method and residual method [39]. The direct method of estimation is to add the unknown parameter PCV into the observation equation and solve it together with other parameters to be solved. Although the physical meaning is clear, the data calculation is large.

In the process of orbit determination, the residual method uses the carrier phase residual under different azimuth and elevation angles to model, and builds the final PCV model by several iterations. Although PCV will be affected by other parameters in the orbit determination process, most of the PCV errors will be reflected in the carrier phase residual. The LEO antenna is divided into a different resolution ($n^\circ \times n^\circ$) grid space, and the average value of phase residual in the range of $\pm n^\circ / 2$ is calculated with the grid node as the center. Because the data are not evenly distributed in the grid space, there is no residual value in some areas, and the PCV value of the grid point cannot be obtained. In order to avoid the "void" phenomenon, the PCV of this part of grid points is assigned a value of 0, and the complete PCV model can be obtained. The observed residual is affected by the clock offset, and the influence of this error is mitigated through multiple iterations, typically requiring 3–5 iterations to achieve convergence.

The satellite-borne GPS data from the HY-2B and HY-2C satellites collected between 14 and 20 December 2020, as well as data from HY-2D satellite from 20 to 26 September 2021, were used to estimate the PCV model by using the direct method and residual method, and the results are shown in Figure 6. Upon comparing the PCV models derived from these two different methods, it becomes apparent that they exhibit similar distribution characteristics, yet some differences are discernible. The direct method involves solving for the PCV at individual grid points as unknown parameters, leading to a more precise estimation of PCV. Consequently, the PCV map resulting from this method displays a speckled distribution. On the other hand, the residual method for PCV estimation entails averaging the residual errors across the grid space. As a result, the PCV values at adjacent grid points tend to be more similar, and the PCV map is characterized by a striped distribution.

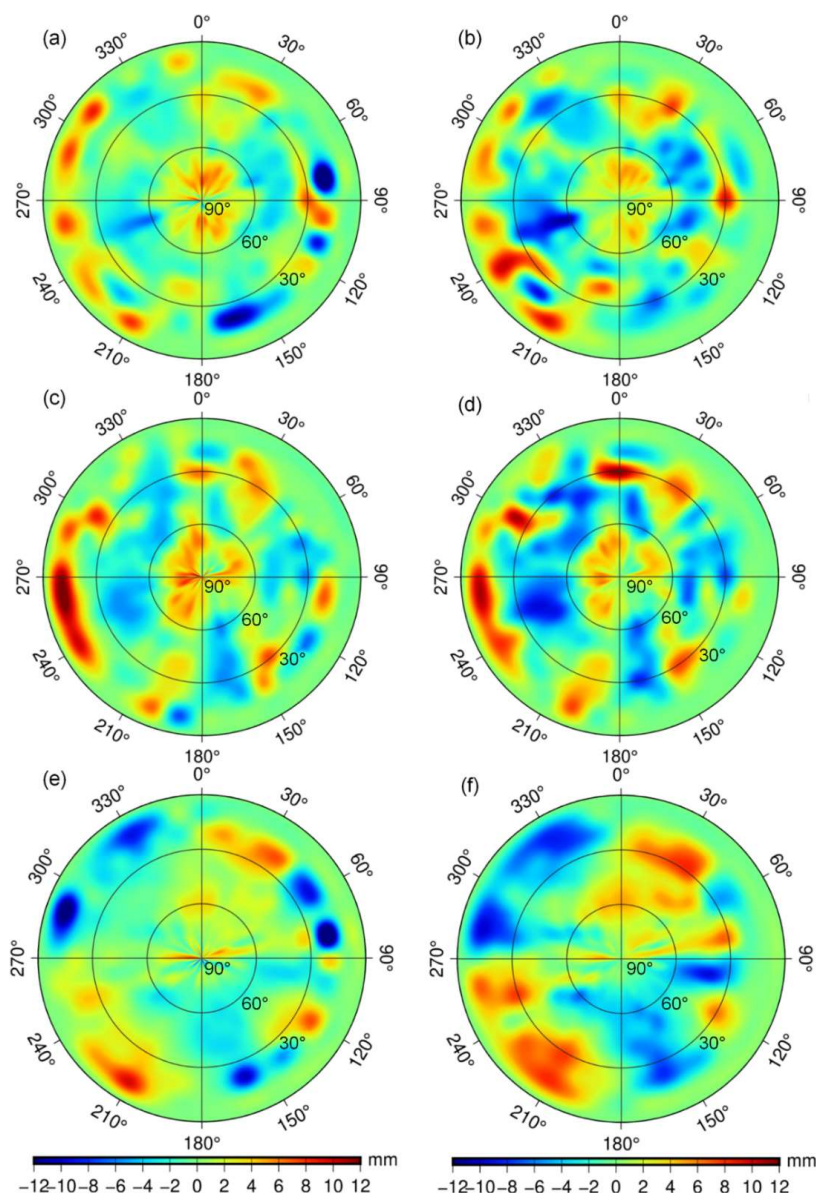


Figure 6. PCV model ((a) HY-2B Residual method PCV model, (b) HY-2B Direct method PCV model, (c) HY-2C Residual method PCV model, (d) HY-2C direct method PCV model, (e) HY-2D Residual method PCV model, (f) HY-2D Direct method PCV model).

As shown in Table 5, after adding the PCV model, the orbit determination accuracy is improved. The carrier phase residual is reduced by 0.4~0.6 mm, and the 3D RMS of the reduced-dynamic orbit to CNES orbit intercomparison was reduced by 0.2~0.3 cm. The direct estimation method is to solve the PCV value of each grid. When the PCV model with a higher resolution is estimated, the calculation is large and the time required is long. As a post-processing method, the residual method has high computational efficiency and is similar to the PCV model estimated by the direct method. The improvement of orbit determination accuracy is basically the same. Considering both computational efficiency and accuracy, this paper opts for the residual method to estimate the PCV model for reduced-dynamic precision orbit determination.

Table 5. Average carrier phase residual RMS value and orbit 3D RMS after PCV model is added.

Type of Orbit	Carrier Phase Residual (mm)	RD Orbit 3D RMS (cm)
HY-2B_noPCV	8.3	3.11
HY-2B_Residual method	7.9	2.91
HY-2B_Direct method	7.9	2.91
HY-2C_noPCV	7.9	3.04
HY-2C_Residual method	7.4	2.81
HY-2C_Direct method	7.3	2.80
HY-2D_noPCV	8.5	3.23
HY-2D_Residual method	8.0	2.89
HY-2D_Direct method	8.0	2.90

4.3. Analysis of Orbit Accuracy

The accuracy of orbit determination can be effectively reflected by reasonable validation of orbit determination results. The accuracy evaluation methods mainly include internal coincidence checking and external coincidence checking. In this section, the internal validations accuracy of the reduced-dynamic orbit is evaluated using the overlapping orbit validation, and the external accuracy is evaluated by the comparison with the CNES orbit, SLR validation, and SLR three-dimensional validation. These validation procedures collectively provide a comprehensive assessment of the accuracy and reliability of the orbit determination results.

(1) Overlapping orbit validation

Overlap orbit validation is performed to compare the results of two independent orbit determination, which can initially reflect the accuracy and stability of orbit determination. The data from one day are divided into two arcs for orbit determination, and the periods are 00:00~15:00 and 09:00~24:00, respectively. Because of the two independent orbit determination processes, the orbit determination results can be considered to be unrelated. At the same time, in order to avoid the boundary effect, the overlapping arcs from 10:00 to 14:00 are selected for comparison.

Table 6 shows the comparative results of seven overlapping arcs in R, T, N, and 3D directions during the HY-2B/2C/2D satellite constellation experiment. It can be seen that the accuracy in the R and N directions is the same, the RMS value in the T direction is significantly greater than that in the R and N directions, and the 3D RMS is less than 2 cm, indicating that the accuracy of the internal validation in the orbit determination is good.

Table 6. Seven-day summary results of overlapping arcs (cm).

	HY-2B			HY-2C			HY-2D		
	R	T	N	R	T	N	R	T	N
Min	-1.21	-2.54	-1.74	-0.95	-3.42	-1.37	-1.15	-2.75	-1.03
Max	1.78	2.79	1.56	1.43	2.63	1.23	1.28	1.98	1.29
Mean	0.24	0.31	-0.26	0.15	-0.26	0.11	-0.08	-0.16	0.14
STD	0.70	1.24	0.72	0.69	1.24	0.81	0.81	1.18	0.83
RMS	0.77	1.35	0.79	0.72	1.31	0.83	0.82	1.22	0.86
3D RMS		1.74			1.71			1.70	

(2) Orbit comparison with CNES

To identify and evaluate potential systematic errors in precision orbit determination, a comparison is made with the DORIS precision orbit data provided by CNES. Figure 7

shows the radial, tangential and normal RMS values of the reduced-dynamic (RD) orbit of the HY-2B/2C/2D satellites compared with the CNES orbit. This comparison aids in assessing the consistency and accuracy of the precision orbit determination results.

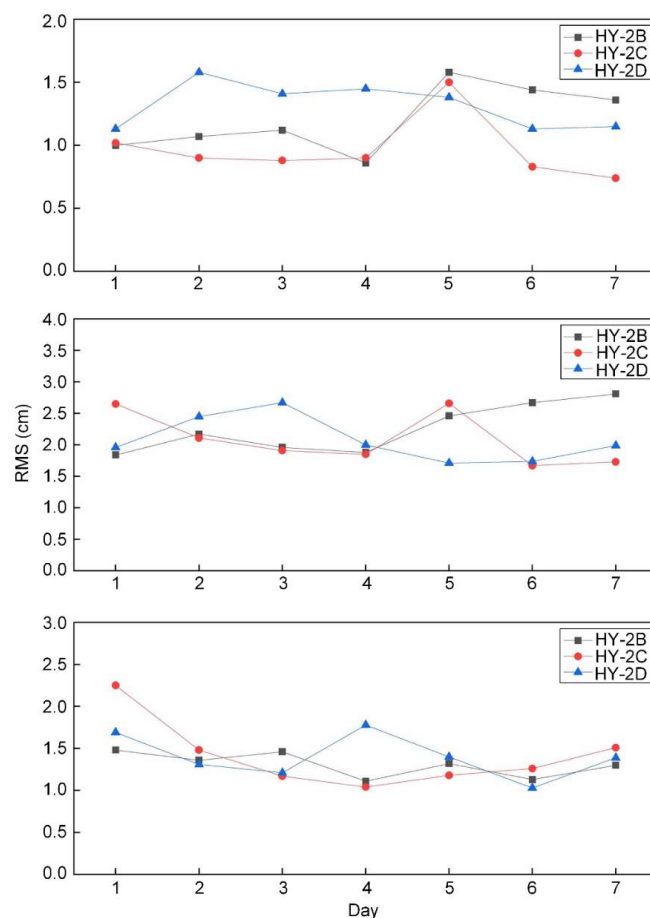


Figure 7. Intercomparison between RD and CNES orbits in the R, T, and N directions.

As can be seen from Figure 7 and Table 7, compared with the orbit provided by CNES, the reduced-dynamic orbits of HY-2B/2C/2D satellites have the best accuracy in the R direction, reaching 1.2 cm, 0.97 cm, and 1.32 cm, respectively, and the 3D RMS are 2.88 cm, 2.75 cm, and 2.85 cm, respectively. The fluctuation range of the RMS value in the R direction is 0.74~1.58 cm, in the T direction 1.67~2.81 cm, and in the N direction 1.03~2.25 cm, and the fluctuation range in the R direction is the smallest. The 3D accuracy of HY-2B/2C/2D satellites is less than 3 cm, which can fully meet the needs of high-precision satellite orbit determination.

Table 7. Statistics of intercomparison results between RD and CNES orbits (cm).

	HY-2B			HY-2C			HY-2D		
	R	T	N	R	T	N	R	T	N
Min	-3.06	-3.83	-3.48	-3.21	-4.01	-2.91	-3.57	-4.17	-3.68
Max	3.21	4.35	3.47	3.03	3.97	3.67	3.25	3.35	3.36
Mean	0.23	0.11	0.05	-0.07	-0.06	0.13	-0.13	-0.21	-0.03
STD	1.17	2.18	1.31	0.97	2.08	1.40	1.31	2.02	1.40
RMS	1.20	2.26	1.31	0.97	2.08	1.41	1.32	2.07	1.40
3D RMS		2.88			2.75			2.85	

(3) SLR validation

The SLR observation data for HY-2B/2C/2D satellites, made available by the International Laser Ranging Service Organization, was used to perform an external coincidence accuracy check of the orbit. This involved comparing the distances calculated from SLR data to the LEO with the distances obtained from the orbit determination results, and the difference between the two was statistically analyzed [40]. It is important to note that the accuracy of SLR station coordinates plays a significant role in the validation results [41]. The International Laser Ranging Service (ILRS) has published SLR2008 and SLRF2020, and the experiment reveals that the coordinates of SLR station are calculated using the two sources to have centimeter-level disagreements in the x and y directions, and millimeter-level disagreements in the z direction. The differences in coordinates between SLR2008 and SLRF2020 files are a combined result of various factors, which may include crustal movement, mass redistribution, station maintenance, and other causes. Since SLRF2020 is the latest version, incorporating updated station positions and velocities, this study utilizes the SLRF2020 model for SLR range validation.

Data quality varies from SLR station due to the different surroundings and technical hardware. Therefore, we not only tally all SLR validation results but also select a number of high-quality SLR stations (called core stations) based on the Monthly GLOBAL report cards published by ILRS to provide more reliable SLR validation results. The Normal Point (NP) data, published by the ILRS, are generated following the conclusion of the laser pass and are typically transmitted to the ILRS within hours of observation. NP data undergo preprocessing, which includes the removal of obvious erroneous data and the exclusion of outliers caused by equipment malfunctions or other anomalies. These core stations (including Yarragadee and Mount Stromlo stations in Australia; Matera MLRO stations in Italy; Potsdam and Wettzell stations in Germany; Graz stations in Austria; Herstmonceux stations in the United Kingdom; Haleakala, Greenbelt, and Monument Peak stations in the United States; and Zimmerwald Station in Switzerland) provided 66% of NP data.

The statistics of the HY-2B/2C/2D satellite observation data relative to the global SLR station are shown in Figure 8. Station 7090 in Australia provided the most NP data, and observations were made every day during the experiment. During DOY349-355 in 2020, 15 SLR stations tracked the HY-2B satellite, with a total of 876 NP data, 7090 and 7237 stations have observation data every day, and these two stations have a total of 392 NP data, 7403 station has the least amount of NP data. There are 15 SLR stations tracking the HY-2C satellite, with a total of 978 NP data, 7090 and 7237 stations have observation data every day, and these two stations have a total of 410 NP data, and 1834 station has the least NP data. During the period of DOY263-269 in 2021, 19 SLR stations tracked the HY2D satellite, with a total of 1456 NP data. The HY2D satellite was continuously observed by stations 7090, 7810, 7825, and 7941.

Table 8 shows the SLR validation results. If only the core station observation data are used, the RMS values of the HY-2B/2C/2D reduced-dynamic orbit SLR validation are 2.34 cm, 2.40 cm, and 2.31 cm, respectively. If NP data from all stations are used, the RMS values are within 3.5 cm. The experimental results show that the “HY2_Receiver” demonstrates stable performance and can reliably receive high-quality data, effectively meeting the requirements for high-precision orbit determination.

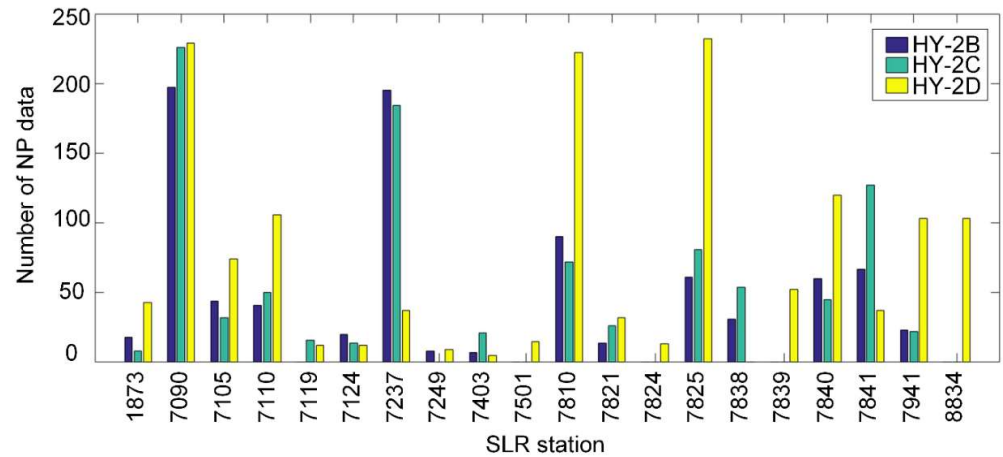


Figure 8. NP data quantity of SLR station.

Table 8. SLR validate residuals at core stations and all stations (cm).

Satellite	Core Stations	All Stations
HY-2B	2.34	3.25
HY-2C	2.40	3.24
HY-2D	2.31	3.34

(4) SLR 3D validation

Since the SLR validation results can only reflect the distance error and cannot evaluate the orbit accuracy from the three directions of R, T, and N, this study obtained the orbit accuracy evaluation in the three directions based on the SLR validation and the error propagation law [42]. SLR stations with more than 50 NP data are selected for experiments, and the results are shown in Table 9.

Table 9. Summary of SLR 3D validation results (cm).

SLR Station	HY-2B				HY-2C				HY-2D			
	R	T	N	3D	R	T	N	3D	R	T	N	3D
7090	0.82	1.32	0.83	1.76	1.36	1.79	1.32	2.61	1.27	1.56	1.54	2.53
7105	-	-	-	-	-	-	-	-	1.89	2.43	1.75	3.54
7110	-	-	-	-	1.89	2.49	2.05	3.74	1.45	1.98	1.51	2.88
7237	1.73	2.36	1.68	3.37	1.97	2.35	1.65	3.48	-	-	-	-
7810	0.86	1.22	0.79	1.69	1.01	1.35	1.22	2.08	0.92	1.35	0.91	1.87
7825	1.45	1.98	1.13	2.70	0.94	1.68	1.12	2.22	1.01	1.48	0.97	2.04
7838	-	-	-	-	1.76	3.01	1.65	3.86	-	-	-	-
7839	-	-	-	-	-	-	-	-	1.54	2.08	1.62	3.05
7840	1.15	1.38	1.43	2.30	-	-	-	-	1.37	1.54	1.68	2.66
7841	0.87	1.29	1.10	1.91	1.23	1.10	0.92	1.89	0.98	1.25	1.11	1.94
7941	-	-	-	-	-	-	-	-	1.54	2.15	1.48	3.03
8834	-	-	-	-	-	-	-	-	1.62	2.39	1.85	3.43
Total	1.20	1.65	1.20	2.37	1.50	2.06	1.46	2.94	1.39	1.87	1.48	2.76

As can be seen from Table 9, SLR three-dimensional validation results are similar to CNES orbit intercomparison results, and 3D RMS are greater than SLR core station inspection errors, but smaller than all SLR station inspection errors. This is because most of the stations with more than 50 NP data are core stations. The SLR three-dimensional validation method can evaluate orbit accuracy more directly.

5. Conclusions

In this paper, a seven-day dataset of HY-2B/2C/2D satellite-borne GPS data was carefully selected for analysis. Initially, data quality was assessed, taking into consideration factors such as satellite visibility, data integrity rate, multipath error, and elevation angle, among others. Subsequently, the phase center variation (PCV) model was estimated using both the direct method and the residual method. Finally, precision orbit determination was executed using the reduced dynamic method, and the accuracy of the orbit determination results was rigorously scrutinized through overlapping orbit validation, an orbit comparison with CNES, SLR validation, and SLR 3D validation.

- (1) The “HY2_Receiver” demonstrated exceptional data quality, with 95.5% of epochs observing five or more satellites. The data loss rates for L1 and L2 bands were 3% and 5.5%, respectively, and the average RMS for MP1 and MP2 were 0.36 m meters and 0.24 m, respectively.
- (2) The estimation of the PCV model using both the direct and residual methods yielded nearly identical results when applied to orbit determination. This led to a reduction in the carrier phase residual by 0.4 to 0.6 mm during orbit determination. When compared with the CNES orbit, the 3D RMS was reduced by 3 to 4 mm, signifying a substantial enhancement in orbit determination accuracy.
- (3) The internal accuracy validation was conducted through overlapping orbit assessment, and the 3D RMS of the overlapping arc consistently remained within 2 cm. Comparisons with CNES-provided orbits revealed 3D RMS values within 3 cm. The selection of SLR core stations, based on the Monthly GLOBAL report cards from ILRS, led to validation accuracies within 2.5 cm. The validation accuracy of all SLR NP data was within 3.5 cm. The SLR three-dimensional validation method was used to evaluate the orbit, with results in the R, T, and N directions mirroring those of the CNES orbit intercomparison, and a 3D RMS of less than 3 cm.

Author Contributions: Methodology, X.J. and G.W.; software, G.W.; validation, X.J. and J.G.; formal analysis, G.W., X.J., and J.G.; investigation, X.C.; data curation, G.W.; writing—original draft, X.J. and G.W.; writing—review and editing, J.G.; visualization, H.P.; supervision, Y.J. and H.P.; funding acquisition, J.G. and X.J. All authors have read and agreed to the published version of the manuscript.

Funding: This research was funded by National Natural Science Foundation of China (grant Nos. 42274006, 42192535, and 42242015), and the Postdoctoral Fellowship Program of China Postdoctoral Science Foundation (Grant No. GZC20231019).

Data Availability Statement: Satellite-borne GPS data are obtained from the NSOAS (<https://osdds.nsoas.org.cn>). GPS satellite orbits, clocks, and Earth rotation parameters are provided by the CODE (<ftp://ftp.aiub.unibe.ch/CODE> (accessed on 1 January 2020)). SLR station data and SLR tracking data are obtained from ILRS (<https://cddis.nasa.gov/archive/slr/products/resource/> (accessed on 1 January 2020)); https://ilrs.gsfc.nasa.gov/network/system_performance/global_report_cards (accessed on 1 January 2020)). CNES precise orbit ephemeris data are downloaded from CNES (<https://aviso-data-center.cnes.fr/>).

Acknowledgments: Our sincere thanks go to the CODE for providing GPS satellite orbits, clocks and Earth rotation parameters, the ILRS for providing SLR station data and SLR tracking data, and the CNES for providing HY-2B/2C/2D precise orbit ephemeris data. This study is partially supported by the National Natural Science Foundation of China (grant Nos. 42274006, 42192535, and 42242015), and the Postdoctoral Fellowship Program of China Postdoctoral Science Foundation (Grant No. GZC20231019).

Conflicts of Interest: The authors declare no conflicts of interest.

References

1. Yu, R.; Lu, H.; Li, S.; Zhu, D.; Zhou, W.; Dang, P.; Wang, C.; Jin, X.; Lv, R.; Li, H. Instrument design and early in-orbit performance of HY-2B scanning microwave radiometer. *IEEE T Geosci. Remote* **2021**, *60*, 1–13. [[CrossRef](#)]
2. Fang, Q.; Guo, W.; Wang, C. Time tag bias correction of HY-2 satellite altimeter by in-orbit calibration using reconstructive transponder. *Int. J. Remote Sens.* **2025**, 1–14. [[CrossRef](#)]
3. Jayles, C.; Vincent, P.; Rozo, F.; Balandraud, F. DORIS-DIODE: Jason-1 has a navigator on board. *Mar. Geod.* **2004**, *27*, 753–771. [[CrossRef](#)]
4. Bury, G.; Sosnica, K.; Zajdel, R. Multi-GNSS orbit determination using satellite laser ranging. *J. Geod.* **2019**, *93*, 2447–2463. [[CrossRef](#)]
5. Kang, Z.; Bettadpur, S.; Nagel, P.; Save, H.; Poole, S.; Pie, N. GRACE-FO precise orbit determination and gravity recovery. *J. Geod.* **2020**, *94*, 85. [[CrossRef](#)]
6. Bertiger, W.I.; Bar-Sever, Y.E.; Christensen, E.J.; Davis, E.S.; Guinn, J.R.; Haines, B.J.; Yunck, T.P. GPS precise tracking of TOPEX/POSEIDON: Results and implications. *J. Geophys. Res.-Oceans* **1994**, *99*, 24449–24464. [[CrossRef](#)]
7. Guo, H.; Guo, J.; Yang, Z.; Wang, G.; Qi, L.; Lin, M.; Ji, B. On satellite-borne GPS data quality and reduced-dynamic precise orbit determination of HY-2C: A case of orbit validation with onboard DORIS data. *Remote Sens.* **2021**, *13*, 4329. [[CrossRef](#)]
8. Huang, W.; Männel, B.; Sakic, P.; Ge, M.; Schuh, H. Integrated processing of ground- and space-based GPS observations: Improving GPS satellite orbits observed with sparse ground networks. *J. Geod.* **2020**, *94*, 104. [[CrossRef](#)]
9. Prange, L.; Orliac, E.; Dach, R.; Arnold, D.; Beutler, G.; Schaer, S.; Jaggi, A. CODE's five-system orbit and clock solution—The challenges of multi-GNSS data analysis. *J. Geod.* **2017**, *91*, 345–360. [[CrossRef](#)]
10. Švehla, D.; Rothacher, M. Kinematic positioning of LEO and GPS satellites and IGS stations on the ground. *Adv. Space Res.* **2005**, *36*, 376–381. [[CrossRef](#)]
11. Kang, Z.; Tapley, B.; Bettadpur, S.; Ries, J.; Nagel, P.; Pastor, R. Precise orbit determination for the GRACE mission using only GPS data. *J. Geod.* **2006**, *80*, 322–331. [[CrossRef](#)]
12. Wang, Z.; Li, Z.; Wang, L.; Wang, N.; Yang, Y.; Li, R.; Zhang, Y.; Liu, A.; Yuan, H.; Hoque, M. Comparison of the real-time precise orbit determination for LEO between kinematic and reduced-dynamic modes. *Measurement* **2022**, *187*, 110224. [[CrossRef](#)]
13. Wang, Y.C.; Li, M.; Jiang, K.C.; Li, W.W.; Qin, G.E. Reduced-dynamic precise orbit determination of Haiyang-2B altimetry satellite using a refined empirical acceleration model. *Remote Sens.* **2021**, *13*, 3702. [[CrossRef](#)]
14. Montenbruck, O.; Kroes, R. In-flight performance analysis of the CHAMP BlackJack GPS Receiver. *GPS Solut.* **2003**, *7*, 74–86. [[CrossRef](#)]
15. Tao, Y.; Liu, C.; Liu, C.Y.; Zhao, X.; Hu, H. Empirical wavelet transform method for GNSS coordinate series denoising. *J. Geovisual. Spatial Anal.* **2021**, *5*, 9. [[CrossRef](#)]
16. Hwang, C.; Tseng, T.P.; Lin, T.H.; Švehla, D.; Hugentobler, U. Quality assessment of FORMOSAT-3/COSMIC and GRACE GPS observables: Analysis of multipath, ionospheric delay, and phase residual in orbit determination. *GPS Solut.* **2010**, *14*, 121–131. [[CrossRef](#)]
17. Jäggi, A.; Dach, R.; Montenbruck, O.; Hugentobler, U.; Bock, H.; Beutler, G. Phase center modeling for LEO GPS receiver antennas and its impact on precise orbit determination. *J. Geod.* **2009**, *83*, 1145–1162. [[CrossRef](#)]
18. Schreiter, L.; Montenbruck, O.; Zangerl, F.; Siemes, C.; Arnold, D.; Jaggi, A. Bandwidth correction of swarm GPS carrier phase observations for improved orbit and gravity field determination. *GPS Solut.* **2021**, *25*, 70. [[CrossRef](#)] [[PubMed](#)]
19. Jin, B.; Li, Y.Q.; Jiang, K.C.; Li, Z.L.; Chen, S.S. GRACE-FO antenna phase center modeling and precise orbit determination with single receiver ambiguity resolution. *Remote Sens.* **2021**, *13*, 4204. [[CrossRef](#)]
20. Xia, Y.; Liu, X.; Guo, J.; Yang, Z.; Qi, L.; Ji, B.; Chang, X. On GPS data quality of GRACE-FO and GRACE satellites: Effects of phase center variation and satellite attitude on precise orbit determination. *Acta Geod. Geophys.* **2021**, *56*, 93–111. [[CrossRef](#)]
21. Wang, Y.; Guo, J.; Ya, S.; Jia, Y.; Guo, H.; Chang, X.; Liu, X. Impact of Pseudo-Stochastic Pulse and Phase Center Variation on Precision Orbit Determination of Haiyang-2A from Experimental HY2 Receiver GPS Data. *Remote Sens.* **2024**, *16*, 1336. [[CrossRef](#)]
22. Peng, H.; Zhou, C.; Zhong, S.; Peng, B.; Zhou, X.; Yan, H.; Zhang, J.; Han, J.; Guo, F.; Chen, R. Analysis of precise orbit determination for the HY-2D satellite using onboard GPS/BDS observations. *Remote Sens.* **2022**, *14*, 1390. [[CrossRef](#)]
23. Tseng, T.P.; Hwang, C.; Yang, S.K. Assessing attitude error of FORMOSAT-3/COSMIC satellites and its impact on orbit determination. *Adv. Space Res.* **2012**, *49*, 1301–1312. [[CrossRef](#)]
24. Abou Galala, M.; Kaloop, M.R.; Rabah, M.M.; Zeidan, Z.M. Improving precise point positioning convergence time through TEQC multipath linear combination. *J. Surv. Eng.* **2018**, *144*, 04018002. [[CrossRef](#)]
25. Guo, J.; Qi, L.; Liu, X.; Chang, X.; Ji, B.; Zhang, F. High-order ionospheric delay correction of GNSS data for precise reduced-dynamic determination of LEO satellite orbits: Cases of GOCE, GRACE, and SWARM. *GPS Solut.* **2023**, *27*, 13. [[CrossRef](#)]
26. Estey, L.H.; Meertens, C.M. TEQC: The multi-purpose toolkit for GPS/GLONASS data. *GPS Solut.* **1999**, *3*, 42–49. [[CrossRef](#)]
27. Mao, X.Y.; Arnold, D.; Girardin, V.; Villiger, A.; Jäggi, A. Dynamic GPS-based LEO orbit determination with 1 cm precision using the Bernese GNSS Software. *Adv. Space Res.* **2021**, *67*, 788–805. [[CrossRef](#)]

28. Zhang, B.B.; Wang, Z.T.; Zhou, L.; Feng, J.; Qiu, Y.D.; Li, F.P. Precise orbit solution for Swarm using space-borne GPS data and optimized pseudo-stochastic pulses. *Sensors* **2017**, *17*, 635. [[CrossRef](#)]
29. Švehla, D.; Rothacher, M. Kinematic and reduced-dynamic precise orbit determination of low earth orbiters. *Adv. Geosci.* **2003**, *1*, 47–56. [[CrossRef](#)]
30. Wang, Y.; Li, M.; Jiang, K.; Li, W.; Zhao, Q.; Peng, H.; Lin, M. Precise orbit determination of the Haiyang-2C altimetry satellite using attitude modeling. *GPS Solut.* **2022**, *26*, 35. [[CrossRef](#)]
31. Springer, T.A.; Beutler, G.; Rothacher, M. Improving the orbit estimates of GPS satellites. *J. Geod.* **1999**, *73*, 147–157. [[CrossRef](#)]
32. Jäggi, A.; Hugentobler, U.; Beutler, G. Pseudo-stochastic orbit modeling techniques for low-earth orbiters. *J. Geod.* **2006**, *80*, 47–60. [[CrossRef](#)]
33. Beutler, G.; Jäggi, A.; Hugentobler, U.; Mervart, L. Efficient satellite orbit modelling using pseudo-stochastic parameters. *J. Geod.* **2006**, *80*, 353–372. [[CrossRef](#)]
34. Chen, J.P.; Wang, J.X. Reduced-dynamic precise orbit determination for low earth orbiters based on Helmert transformation. *Artif. Satell.* **2007**, *42*, 155–165. [[CrossRef](#)]
35. Rodriguez-Solano, C.; Hugentobler, U.; Steigenberger, P. Adjustable box-wing model for solar radiation pressure impacting GPS satellites. *Adv. Space Res.* **2012**, *49*, 1113–1128. [[CrossRef](#)]
36. Zingerle, P.; Pail, R.; Gruber, T.; Oikonomidou, X. The combined global gravity field model XGM2019e. *J. Geod.* **2020**, *94*, 66. [[CrossRef](#)]
37. Ivantsov, A.V. Dynamical model of motion for asteroids based on the DE405 theory. *Kinemat. Phys. Celest. Bodies* **2007**, *23*, 65–69. [[CrossRef](#)]
38. Lyard, F.H.; Allain, D.J.; Cancet, M.; Carrere, L.; Picot, N. FES2014 global ocean tide atlas: Design and performance. *Ocean Sci.* **2021**, *17*, 615–649. [[CrossRef](#)]
39. Lu, C.; Zhang, Q.; Zhang, K.; Zhu, Y.; Zhang, W. Improving LEO precise orbit determination with BDS PCV calibration. *GPS Solut.* **2019**, *23*, 109. [[CrossRef](#)]
40. Zajdel, R.; Sošnica, K.; Bury, G. A new online service for the validation of multi-GNSS orbits using SLR. *Remote Sens.* **2017**, *9*, 1049. [[CrossRef](#)]
41. Guo, J.; Wang, Y.; Shen, Y.; Liu, X.; Sun, Y.; Kong, Q. Estimation of SLR station coordinates by means of SLR measurements to kinematic orbit of LEO satellites. *Earth Planets Space* **2018**, *70*, 201. [[CrossRef](#)]
42. Guo, J.; Wang, G.; Guo, H.; Lin, M.; Peng, H.; Chang, X.; Jiang, Y. Validating precise orbit determination from satellite-borne GPS data of Haiyang-2D. *Remote Sens.* **2022**, *14*, 2477. [[CrossRef](#)]

Disclaimer/Publisher’s Note: The statements, opinions and data contained in all publications are solely those of the individual author(s) and contributor(s) and not of MDPI and/or the editor(s). MDPI and/or the editor(s) disclaim responsibility for any injury to people or property resulting from any ideas, methods, instructions or products referred to in the content.